TORQUE AND ROTATION RATE OF THE BACTERIAL FLAGELLAR MOTOR

P. LÄUGER
Department of Biology, University of Konstanz, D-7750 Konstanz, Federal Republic of Germany

ABSTRACT This paper describes an analysis of microscopic models for the coupling between ion flow and rotation of bacterial flagella. In model I it is assumed that intersecting half-channels exist on the rotor and the stator and that the driving ion is constrained to move together with the intersection site. Model II is based on the assumption that ion flow drives a cycle of conformational transitions in a channel-like stator subunit that are coupled to the motion of the rotor. Analysis of both mechanisms yields closed expressions relating the torque M generated by the flagellar motor to the rotation rate ν. Model I (and also, under certain assumptions, model II) accounts for the experimentally observed linear relationship between M and ν. The theoretical equations lead to predictions on the relationship between rotation rate and driving force which can be tested experimentally.

INTRODUCTION

Many bacteria use rotating flagella for locomotion (1–8). The force driving the rotation of the flagellum is generated in the basal body, which is embedded in the cell wall and the plasma membrane. The basal body of gram-positive bacteria such as *Bacillus subtilis* contains two parallel rings of 20–30-nm diam. The M ring is co-planar with the plasma membrane and is assumed to be rigidly attached to the flagellum. The S ring is located on the external side of the plasma membrane and is likely to be connected with the cell wall. It is usually assumed that the torque required for the movement of the flagellum is generated by rotation of the M ring relative to the S ring. Gram-negative bacteria such as *Escherichia coli* have two additional rings which are associated with the peptidoglycan layer and the outer lipopolysaccharide membrane; they probably serve as bearings and do not participate in force generation.

The flagellar motor contains several independent force-generating units. This notion is based on experiments with paralyzed *mot* mutants of *E. coli* (9, 10), in which induction of the synthesis of the *mot* B protein leads to a stepwise increase of rotation speed. From the ratio of the maximal speed to the size of the speed increment, the existence of about 16 independent units can be inferred (10). This conclusion is consistent with the results of electron microscopic studies (11) which gave evidence for 16-fold rotational symmetry in the M ring. In freeze-fracture electron micrographs of the gram-negative bacterium *Aquaspirillum serpens*, a similar number (14–16) of membrane particles ("studs") is seen at the periphery of annular depressions, normally occupied by one of the rings (12). The *mot* proteins are not found in preparations of isolated basal bodies but remain with the cytoplasmic membrane (13).

Numerous studies have shown that in *E. coli* and in a number of other bacteria the motor is driven by a transmembrane electrochemical gradient of H^+ (14–20). In alkalophilic bacteria the driving ion seems to be Na^+ (21). It has been estimated that at a driving force of 100–200 mV, the passage of a few hundred protons per revolution is sufficient to sustain rotation of the motor at high viscous load (22). When the load is heavy, the motor operates at constant torque, the rotation rate being inversely proportional to the viscosity of the medium (18, 23). When the load is light, as, for instance, in a filament-less mutant, the motor runs at a constant limiting rate, independent of the load (7, 24). The motor can switch from clockwise to counterclockwise rotation and it can be driven artificially by a protonmotive force of reverse polarity (18).

Several hypothetical mechanisms for the flagellar motor have been proposed (7, 25–37). These models have shown how in principle coupling between ion translocation and rotation can arise, but, except for the interesting work of Oosawa and collaborators (33–35), they have not been worked out in sufficient detail as to allow a quantitative analysis of the relationship between torque and rotational speed.

In the following, we discuss two kinetic models of the flagellar motor involving transitions between discrete states. The analysis leads to analytical expressions relating rotation rate to electrochemical driving force and to viscous load. This study has been stimulated by recent experimental work from the laboratory of Berg (24) in which the torque M generated by the flagellar motor has been measured in a wide range of rotation rates ν. The results of the theoretical analysis agree with the experimentally observed linear relationship between M and ν. Moreover, predictions on the dependence of ν on driving force can be derived that are amenable to experimental test.

MODEL I: INTERSECTING HALF-CHANNELS

Model I is based on the notion that ion passage through the plasma membrane requires a kind of "channel," i.e., a series of polar ligand groups with which the ion interacts in an energetically favorable way (27, 29). The model is characterized by the following assumptions (Fig. 1): (*a*) The M ring is surrounded by a number of "stator elements" attached to the cell wall, each containing a ligand row oriented perpendicular to the plane of the ring. The *mot* B gene product may be identical with, or be part of, these stator elements. (*b*) At the periphery of the M ring ligand rows are present that are oriented at an angle θ with respect to the ligand rows on the stator elements. (*c*) The interaction energy of the ion with a single ligand row is not sufficient to compensate for the energy required to remove the ion from water, but an energetically favorable situation is given when the ion is located at the site of intersection of the two ligand rows where it has twice as many ligand groups available.

Under these conditions the ion is constrained to move together with the intersection point. For the geometrical arrangement depicted in Fig. 1, ion flow from the external medium to the cytoplasm leads to counterclockwise[1] rotation of the M ring. A similar model has been considered earlier in which the two half-channels were assumed to be located in the opposing faces of the M and the S ring (27). This geometry has become unlikely by the finding that the *mot* A and *mot* B polypeptides do not co-purify with the basal body but remain in the cytoplasmic membrane (13, 29).

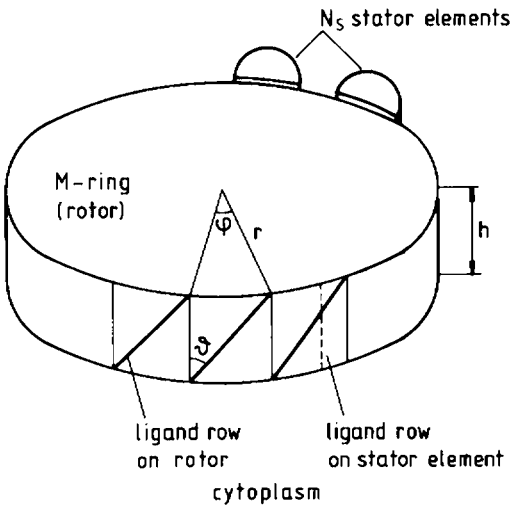

FIGURE 1 Arrangement of ligand rows (half-channels) on rotor and stator. The ligand rows on the circumference of the M ring (rotor) are oriented at an angle θ with respect to the ligand rows on the stator elements. Inward movement of ions occupying the intersection sites leads to counterclockwise rotation of the rotor. r and h are the radius and the height of the ring, respectively.

[1]"Clockwise" and "counterclockwise" refer to the direction of rotation as seen from the extracellular side.

Evaluation of the Rotation Rate

We assume that the oblique ligand rows (or half-channels) on the M ring are narrowly spaced but do not overlap (Fig. 1). If ϕ is the angle subtended by a half-channel, and if h and r are the height and the radius of the ring, the number N_r of half-channels on the periphery of the rotor is given by

$$N_r = \frac{2\pi}{\phi}. \tag{1}$$

We first consider the case that only a single stator element is present at the periphery of the M ring. If the flagellum rotates in a medium of finite viscosity, frictional forces give rise to an (average) external torque m_e which tends to slow down the motor. In the presence of the torque m_e, an ion located in the intersection site experiences a force F_e directed perpendicular to the plane of the ring:

$$F_e = \frac{m_e}{h}\phi = \frac{m_e}{r} tg\,\theta. \tag{2}$$

This relation is derived by the following argument. When an ion in the intersection site is translocated over the distance h (Fig. 1) against a force F_e, work of magnitude $F_e h$ is performed. This work must be equal to the mechanical energy $m_e\phi$ corresponding to rotation of the ring by the angle ϕ. F_e is taken to be positive if the force is directed outward; ϕ and θ are positive when outward movement of ions is associated with clockwise rotation of the flagellum (as in Fig. 1).

The motion of the ion along the half-channel on the stator element, which is coupled to rotation of the ring, may be described by a sequence of discrete steps. For this purpose we introduce the potential energy profile of the ion along the transport pathway, consisting of a series of potential wells separated by activation barriers (Fig. 2). The potential wells are the sites where the ion is energetically favorably surrounded by ligand groups. In the presence of an electric field E and of a mechanical force F_e acting on the proton, the energy level of well $i + 1$, referred to the energy level of well i, changes by the amount ΔU_i:

$$\Delta U_i = -(e_0 E + F_e)a_i. \tag{3}$$

a_i is the distance between potential wells i and $i + 1$, and e_0 is the elementary charge. Implicit in Eq. 3 is the assumption that the electric field strength $E = (\psi' - \psi'')/h$ is constant along the transport pathway. According to the theory of absolute reaction rates (38), the jumping frequencies k_i' and k_i'' of the ion (Fig. 3) are related to ΔU_i in the following way:

$$k_i' = \tilde{k}_i' \exp(-\Delta U_i/2kT) = \tilde{k}_i' \exp[\alpha_i(u + w)/2] \tag{4}$$

$$k_i'' = \tilde{k}_i'' \exp(\Delta U_i/2kT) = \tilde{k}_i'' \exp[-\alpha_{i-1}(u + w)/2] \tag{5}$$

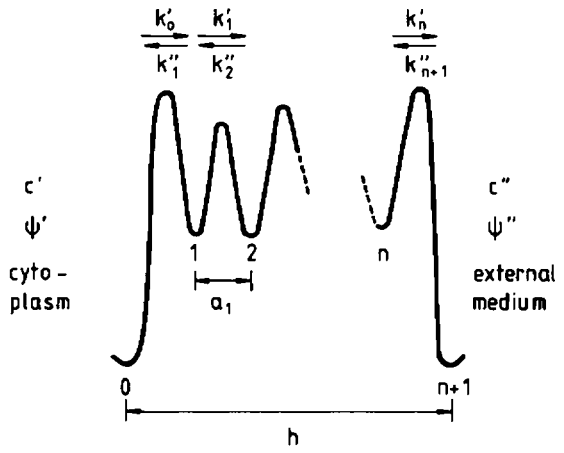

FIGURE 2 Potential-energy profile of the ion along the half-channel on the stator element. c' and c'' are the proton concentrations on the cytoplasmic and the external side of the M ring, respectively, ψ' and ψ'' the electric potentials and k'_0, k'_1, ... the rate constants for crossing the barriers.

$$u = \frac{\psi' - \psi''}{kT/e_0} \tag{6}$$

$$w \equiv \frac{F_c h}{kT} = \frac{m_c \phi}{kT}. \tag{7}$$

$\alpha_i = a_i/h$ is the fractional distance between potential wells i and $i + 1$; for equally spaced wells, the α_i are equal to $1/(n + 1)$. u is the transmembrane voltage in units of $kT/e_0 \approx 25.2$ mV (at 20°C), w the mechanical energy of rotation by angle ϕ against the torque m_c (in units of kT), and $\tilde{k}'_i$ and $\tilde{k}''_i$ are the values of k'_i and k''_i for $u = w = 0$.

Implicit in Eqs. 4 and 5 is the assumption that the torque m_c is continuously acting on the motor, in the same way as an externally applied torque. This represents an approximation, since in reality m_c results from frictional forces associated with movement of the rotor. At low ion concentration, the behavior of the motor may be influenced by fluctuations in the occupancy of the binding sites. For this reason, we restrict the following analysis to high ion concentrations at which the binding sites are always occupied.

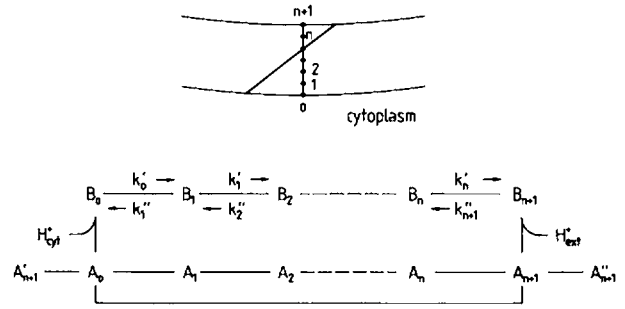

FIGURE 3 Relative motion of the rotor half-channel with respect to the stator half-channel, represented as a sequence of transitions between discrete states. States with empty intersection site are denoted by A, states with occupied intersection by B; A_i and B_i are the states in which the intersection site is located at the position of the ith potential well (Fig. 2). k'_0, k'_1, ... are rate constants of transitions between occupied states.

The relative motion of the rotor with respect to the stator may be described by a sequence of transitions between discrete states. In the reaction scheme of Fig. 3 empty states of the intersection site are denoted by A and occupied states by B; A_i and B_i are the states in which the intersection site is located at the position of the ith energy well (Fig. 2). When the motor performs steady clockwise rotation, the cycle starts in state A_0 by binding of H^+ from the cytoplasm ($A_0 \rightarrow B_0$). The system then moves through $B_1, B_2, \ldots, B_n$ to B_{n+1}. After release of the proton to the external side ($B_{n+1} \rightarrow A_{n+1}$), a transition to state A''_0 takes place in which the next ligand row on the rotor intersects with the ligand row on the stator in position 0. At nonsaturating extracellular proton concentration, cycles with empty binding site ($A_0 \rightarrow A_1 \rightarrow \cdots \rightarrow A_{n+1} \rightarrow A''_0$) will occasionally occur. This represents a loss of strict coupling between proton flux and rotational motion. Close to equilibrium the system carries out a biased random walk among the states of the reaction scheme, corresponding to a superposition of steady rotation and rotary Brownian motion (39). In a motor containing several force-generating units, quasi-continuous rotation occurs already at very small driving force.

For the analysis of the reaction scheme of Fig. 3 we introduce the probability $x[Y]$ that the stator channel is in state Y:

$$\sum_{i=0}^{n+1} \{x[A_i] + x[B_i]\} = 1. \tag{8}$$

Assuming that protonation and deprotonation of the entrance sites ($i = 0$, and $i = n + 1$) are not rate limiting, the probability of states A_0, B_0, A_{n+1}, and B_{n+1} can be expressed by equilibrium dissociation constants K' and K'':

$$\frac{x[B_0]}{x[A_0]} = \frac{c'}{K'}; \qquad \frac{x[B_{n+1}]}{x[A_{n+1}]} = \frac{c''}{K''}. \tag{9}$$

c' and c'' are the proton concentrations in the cytoplasmic and in the extracellular medium, respectively.

When the system is in state A_{n+1}, the rotor half-channel intersects with the external entrance site of the stator half-channel. A transition may then occur to state A''_0 in which the next rotor half-channel intersects with the cytoplasmic entrance site of the stator half-channel; as indicated in Fig. 1 this transition may occur with negligible shift in the angular position of the rotor. Assuming that the energy barrier between states A_{n+1} and A''_0 is low, these states are always in equilibrium with each other:

$$\frac{x[A_{n+1}]}{x[A_0]} = H. \tag{10}$$

(Note that states A_0 and A''_0 are equivalent since all rotor half-channels can be assumed to have identical properties.)

The quantity H is a voltage- and torque-independent equilibrium constant which may be set equal to unity.

According to the principle of microscopic reversibility, the rate constants and equilibrium constants of the reaction cycle of Fig. 3 are connected by the relation

$$\frac{k_0' k_1' \cdot \ldots \cdot k_n'}{k_1'' k_2'' \cdot \ldots \cdot k_{n+1}''} \cdot \frac{K''}{K'H} = \exp(u + w) \tag{11}$$

(see Appendix A). Introducing Eqs. 4 and 5 into Eq. 11 yields

$$\alpha_0 + \alpha_1 + \cdots + \alpha_n = 1. \tag{12}$$

This equation expresses the fact that in the process $A_0 \rightarrow B_0 \rightarrow \cdots \rightarrow B_{n+1} \rightarrow A_{n+1}$, a single elementary charge is translocated across the membrane.

The rotation rate ν of the flagellum is connected with the rate j of ion flux through a single channel. Under the condition that the binding site is always occupied by an ion, j and ν are related by

$$j = N_r \nu. \tag{13}$$

This equation simply states that during one revolution, N_r rotor half-channels pass the stator element. ν is taken to be positive for clockwise rotation of the flagellum (viewed from the extracellular medium); this corresponds, for the geometry shown in Fig. 1, to outward flow of ions ($j > 0$). The flux rate j can be evaluated by calculating the steady-state probabilities $x[Y]$ of the states of the cycle, as described in Appendix B. For $n = 0$, 1, and 2 the rotation rate ν is obtained in the following form, using Eq. 13:

$n = 0$:

$$\nu = \frac{k_1'' H}{N_r K''} \cdot \frac{c' \exp(u + w) - c''}{c'/K' + c'' H/K''} \tag{14}$$

$n = 1$:

$$\nu = \frac{k_1'' k_2'' H}{N_r K''} \cdot \frac{c' \exp(u + w) - c''}{(Q'/K')c' + (Q'' H/K'')c''} \tag{15}$$

$$Q' \equiv k_0' + k_1' + k_1'' \tag{16}$$

$$Q'' \equiv k_1' + k_1'' + k_2'' \tag{17}$$

$n = 2$:

$$\nu = \frac{k_1'' k_2'' k_3'' H}{N_r K} \cdot \frac{c' \exp(u + w) - c''}{(Q'/K')c' + (Q'' H/K'')c''} \tag{18}$$

$$Q' \equiv k_0'(k_1' + k_2' + k_2'') + k_2'(k_1' + k_1'') + k_1'' k_2'' \tag{19}$$

$$Q'' \equiv k_3''(k_1' + k_1'' + k_2'') + k_2'(k_1' + k_1'') + k_1'' k_2''. \tag{20}$$

In the case $n = 0$ the ion passes over a single barrier separating the two entrance sites. For $n > 2$ where the expressions for Q' and Q'' become rather cumbersome, it is preferable calculating j and ν numerically, using Eqs. B1–B3 of Appendix B.

From the derivation of Eqs. 14–20 it is clear that rotation can be driven by a pH difference alone. In this case the driving force is of purely entropic (thermal) origin. When the membrane potential is zero ($u = 0$) and when the motor rotates at vanishing viscous load ($w \approx 0$), the rotation rate ν is simply proportional to the proton concentration difference $c' - c''$ (Eqs. 14, 15, and 18).

Eqs. 14–20 have been derived under the condition that only a single stator element is present. We now assume that the motor contains $N_s \leq N_r$ stator elements which are regularly arranged around the M ring.[2] The external torque m_e per binding site (Eq. 2) and the total external torque M_e acting on the motor are then related by $m_e = M_e/N_s$, so that according to Eqs. 1 and 7, the torque $M = -M_e$ generated by the motor is given by

$$M = -\frac{kT}{2\pi} N_r N_s w. \tag{21}$$

According to the definition of the sign of m_e, $M > 0$ corresponds to counterclockwise rotation of the flagellum.

Following Berg and Khan (30, 31) we assume that the stator elements are elastically coupled to the cell wall so that they can carry out restricted motion along the circumference of the M ring. When a stator element moves by one step while the rotor retains its position, elastic energy is stored which may be released in a subsequent rotation of the rotor. In this way each stator element may act as a (quasi-) independent force-generator. As long as only time-averaged steady-state properties of the motor are considered, the elastic forces acting between the rotor and stator elements need not be taken into account explicitly.

Maximum Torque and Maximum Rotation Rate

In the limit of infinite viscous load, rotation ceases ($\nu = 0$) and the torque M becomes maximal. According to Eqs. 14, 15, or 18, the value w_0 corresponding to $\nu = 0$ is equal to $-u + \ln(c''/c') = -e_0 \Delta p/kT$, where Δp is the protonmotive force acting on the motor:

$$\Delta p = \psi' - \psi'' + \frac{kT}{e_0} \ln \frac{c'}{c''}. \tag{22}$$

This gives

$$M_0 = M_{\nu=0} = \frac{e_0}{2\pi} N_s N_r \Delta p. \tag{23}$$

Eq. 23 has a simple interpretation. $2\pi M_0$ is the work delivered by the motor in a single revolution under near-equilibrium conditions ($\nu \approx 0$). This work is equal to the driving force per ion, $e_0 \Delta p$, times the total number $N = N_r N_s$ of ions that pass through the motor during one revolution.

[2]The condition $N_s \leq N_r$ is introduced to ensure that a stator half-channel intersects not more than once with a rotor half-channel.

Since M_0 is a unique function of Δp, a pH difference ΔpH generates the same maximal torque as a voltage $\Delta\psi = -(kT/e_0)\Delta$pH. This equivalence between $\Delta\psi$ and ΔpH no longer holds at finite rotation rates (see below).

In the limit of vanishing friction, the torque approaches zero and the rotation rate ν becomes maximal. According to Eqs. 14, 15, 18, and 22, this maximal value of ν is given by

$$\nu_0 \equiv \nu_{M=0} = \frac{k_1'' \ldots k_{n+1}'' \, Hc''}{N_r K''} \cdot \frac{\exp(e_0 \Delta p/kT) - 1}{(Q'/K')c' + (Q''H/K'')c''}. \quad (24)$$

ν_0 vanishes with vanishing protonmotive force Δp. On the other hand, from the form of Eq. 24 it is clear that ν_0 is not a unique function of Δp (note that $k_1'', k_2'', \ldots, K', K'', Q'$, and Q'' depend in general on voltage u). This means that (in contrast to the behavior of M_0) a pH difference is, in general, not equivalent to a voltage $\Delta\psi$ with respect to rotation speed. Only close to equilibrium ($c' \approx c''$, $u \approx 0$, $\Delta p \approx 0$) the relation $\nu_0 \propto \Delta p$ holds. It may be expected, however, that for certain combinations of the kinetic parameters an approximate equivalence between $\Delta\psi$ and ΔpH may extend beyond the near-equilibrium range.

Eq. 24 provides a microscopic interpretation for the occurrence of a maximal rotation rate. At low viscous load, rotation speed is limited by the rate constants of the elementary ion-transfer reactions in the motor (33). For instance, for $n = 0$ the maximal rotation rate under the condition $c' = c''$, $K' = K''$, $H = 1$ is equal to $k_1''[\exp(e_0\Delta p/kT) - 1]/N_r$, where k_1'' is the rate constant of ion translocation across the central barrier. The finite rate of the elementary steps in the reaction cycle leads to a kind of intrinsic friction which ultimately limits the speed of the motor. In the vicinity of $\nu = \nu_0$, the motor does not perform work, and all free energy contained in the electrochemical gradient (6 kT per proton at $\Delta p = -150$ mV) is dissipated. The intrinsic friction of the motor may be described by a friction coefficient f_i defined by the relation

$$2\pi\nu_0 f_i = M_0. \quad (25)$$

Comparison with Eqs. 11, 23, and 24 under the condition $|\Delta p| \ll kT/e_0$, $c' = c''$ yields for a channel without internal binding sites ($n = 0$):

$$f_i = \left(\frac{N_r}{2\pi}\right)^2 \frac{kTN_s}{1/k_0' + 1/k_1''}. \quad (26)$$

Analogous expressions can be derived for $n > 0$.

Predicted Values of $M(\nu)$ and Comparison with Experimental Results

Lowe et al. (24) recently described experiments with free-swimming *Streptococcus* cells in media of different viscosities, in which they determined the relationship between torque M and rotation rate ν at large values of ν. Additional information at small rotation rates is provided by experiments with tethered cells (18, 42). Taken together, these studies demonstrate that M varies nearly linearly with ν over virtually the whole range between $\nu \approx 0$ and $\nu_0 \approx 100$ Hz (Fig. 4). $M(\nu)$ can thus be represented by the relation

$$M(\nu) \approx M_0(1 - \nu/\nu_0). \quad (27)$$

M_0 and ν_0 are the maximal torque and the maximal rotation rate introduced in Eqs. 23 and 24.

The predicted form of $M(\nu)$ for $n = 0$, 1, 2, and 7 and different values of the protonmotive force Δp is represented in Fig. 5. For $n \leq 2$, $M(\nu)$ was calculated from Eqs. 14, 15, 18, and 21; for $n = 7$ the matrix-inversion method (43) was used together with Eqs. B1–B3 of Appendix B. It is seen that for increasing number n of internal binding sites, the function $M(\nu)$ approaches a nearly linear behavior. The data of Fig. 4 exclude the models with $n = 0$ and $n = 1$, but, within the experimental error limits, they are compatible with $n \geq 2$. The observed influence of n on $M(\nu)$ agrees with expectation, since for large values of n the potential drop across a single barrier is small so that the dependence of the rate constants on $u + w$ (Eqs. 4 and 5) becomes linear. This point has already been discussed by Lowe et al. (24).

In Fig. 6, M is plotted as a function of ν with the number N_s of stator elements as a variable parameter. This corresponds to the experiment of Block and Berg (10) in which the rotation speed of tethered cells of *mot* B-negative mutants has been recorded during biosynthetic incorporation of the *mot* B protein (a putative constituent of the stator element). As may be expected, $M(\nu)$ curves for

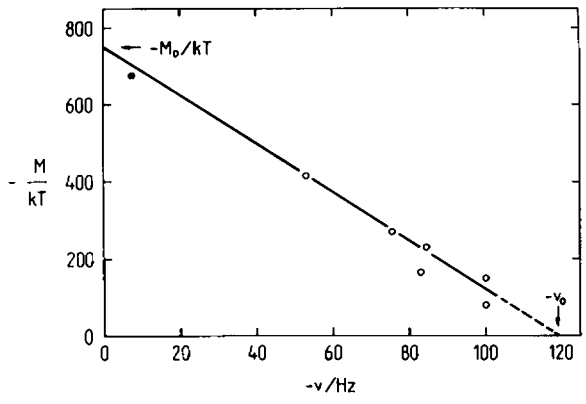

FIGURE 4 Torque M generated by the flagellar motor as a function of rotation rate ν, from Lowe et al. (24). M is referred to a single flagellum and is given in units of $kT \approx 4.1 \cdot 10^{-21}$ J (at 22°C). M and ν are taken to be positive for clockwise rotation of the flagellum (viewed from the extracellular medium). *Open circles*, experiments with free swimming cells of *Streptococcus* in media of different viscosity at 22°C at constant protonmotive force (24). *Solid circle*, experiments with tethered cells (18). At high viscous load ($\nu \approx 0$) the torque approaches a maximum value M_0. At low load ($M \approx 0$) the rotation rate assumes a limiting value ν_0.

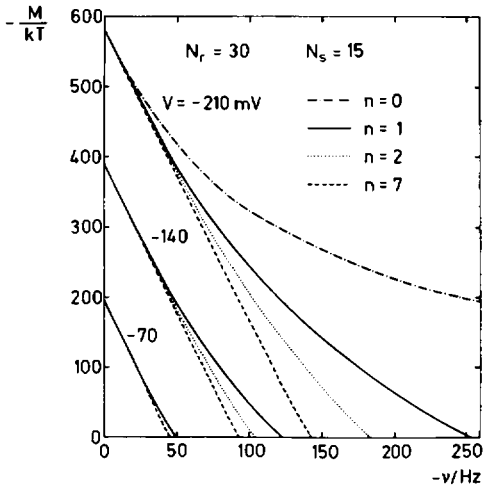

FIGURE 5 Torque M (in units of kT) as a function of rotation rate ν for different values of the protonmotive force Δp. M and ν are taken to be positive for clockwise rotation of the flagellum (viewed from the extracellular medium). n is the number of internal binding sites in the stator half-channel (Fig. 2). $M(\nu)$ has been calculated from Eqs. 14, 15, 18, and 21, or (for $n = 7$) from Eqs. B1–B3. The energy barriers of Fig. 2 have been assumed to be of identical height, so that $\tilde{k}_0' = \tilde{k}_1' = \cdots = \tilde{k}_n' = \tilde{k}'' = \cdots \tilde{k}''_{n+1} \equiv k_0$. The following parameter values have been used for the numerical calculations: $c' = c'' = 10^{-7}$ M; $K' = K'' = 10^{-9}$ M; $H = 1$; $\alpha_i = 1/(n+1)$; $N_r = 30$; $N_s = 15$; $k_0 = 1{,}000\ s^{-1}$ ($n = 0$), $k_0 = 3{,}000\ s^{-1}$ ($n = 1$), $k_0 = 6{,}000\ s^{-1}$ ($n = 2$), $k_0 = 36{,}000\ s^{-1}$ ($n = 7$). The values of the rate constant k_0 have been chosen such that the slope of $M(\nu)$ approximately agrees at $\nu = 0$ for the different values of n. $T = 25$°C.

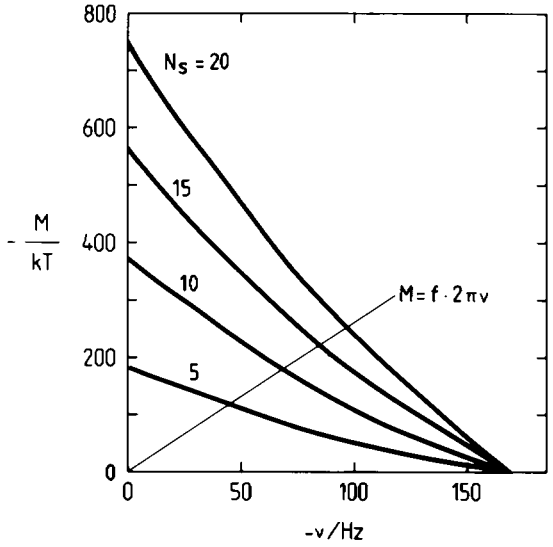

FIGURE 6 Torque M (in units of kT) as a function of rotation rate ν with the number N_s of stator elements as variable parameter. The calculation has been carried out for $n = 2$ using Eqs. 18 and 21 with the following parameter values: $c' = c'' = 10^{-7}$ M; $K' = K'' = 10^{-9}$ M; $H = 1$; $\tilde{k}_0' = \tilde{k}_1' = \tilde{k}_2' = \tilde{k}_1'' = \tilde{k}_2'' = \tilde{k}_3'' = 6{,}000\ s^{-1}$, $\alpha_0 = \alpha_1 = \alpha_2 = 1/3$; $N_r = 30$; $\Delta p = -200$ mV. Values of ν for a given friction coefficient f are specified by the points of intersection of the straight line $M = -f \cdot 2\pi\nu$ with the $M(\nu)$ curves. (The friction coefficient f is defined by $M_e = f \cdot \Omega = -M$, where $\Omega = 2\pi\nu$ is the angular velocity.)

different values of N_s differ in the maximal torque M_0, but pass through the same value of the maximal rotation rate ν_0. Actual values of ν for a given rotational friction coefficient f are specified by the points of intersection of the straight line $M = f \cdot 2\pi\nu$ with the $M(\nu)$ curves. The friction coefficient f is defined by

$$M_e = -f \cdot \Omega, \tag{28}$$

where $M_e = -M$ is torque resulting from frictional forces, and $\Omega = 2\pi\nu$ is the angular velocity.

Introducing $M = 2\pi\nu f$ into Eq. 27 yields, together with Eq. 25:

$$\nu = \frac{\nu_0}{1 + f/f_i}. \tag{29}$$

Thus, for $f \gg f_i$, the rotation rate is proportional to $1/f$, meaning that at high load the motor runs at constant load-independent torque (or constant energy output per revolution). From the experimental results represented in Fig. 4, the intrinsic frictional coefficient of the motor is estimated to be $f_i = M_0/2\pi\nu_0 \simeq 4.0 \cdot 10^{-21}$ J s. This value may be compared with the frictional coefficient f describing the rotation of a tethered cell (24), which is about fifteen times as large ($f \approx 6.0 \cdot 10^{-20}$ J s). On the other hand, from the observation that a filament-free hook spins at about the same speed as an entire flagellum (24) it may be concluded that for a freely spinning flagellum in water the relation $f < f_i$ holds.

According to Eqs. 22 and 23, the maximal torque M_0 is determined, at a given value of Δp, by the product $N_r N_s$, which (for fully occupied binding sites) is equal to the number of protons translocated in one revolution. For physiological values of Δp($\Delta p = -150$ to -200 mV), reasonable assumptions about N_r and N_s ($N_r = 30$–40, $N_s = 15$) yield values of M_0 that approximately agree with the experimental data of Fig. 4. (Assuming that the protonmotive force in the experiments of Fig. 4 was -200 mV, the predicted value of M_0/kT is 760 for $N_r = 40$ and $N_s = 15$.)

In the model discussed here, the maximal rotation rate ν_0 depends on the intrinsic ion-translocation rate constants of the motor (Eq. 24). Estimates of ν_0 from experiments with free-swimming bacteria (24) or with mutants lacking the flagellar filament (7) are in the range of 100–200 Hz. In the simplest version of a symmetrical channel with $n = 2$ ($K' = K''$, $\alpha_1 = \alpha_2 = \alpha_3 = 1/3$, $H = 1$, $\tilde{k}_0' = \tilde{k}_1' = \tilde{k}_2' = \tilde{k}_1'' = \tilde{k}_2'' = \tilde{k}_3'' \equiv k_0$), the maximal rotation rate, as obtained from Eqs. 4, 5, and 24 for $c' = c''$, is given by

$$\nu_0 = \frac{k_0}{4N_r} \cdot \frac{y^6 - 1}{y(1 + y^2 + y^4)} \tag{30}$$

$$y \equiv \exp(e_0\Delta p/6kT) = \exp(u/6).$$

With $\nu_0 = -100$ Hz, $\Delta p = -150$ mV and $N_r = 30$, k_0 is

estimated to be ~5,300 s^{-1}. If a single barrier is rate limiting (rate constant k_0), k_0 would be ~1,500 s^{-1}.

Valuable kinetic information may be obtained by measuring rotation rate as a function of protonmotive force Δp. In experiments with *Streptoccus* (18) and with *Bacillus subtilis* (17, 44) the electrical ($\Delta\psi$) and the chemical (ΔpH) components of Δp were found to be almost equally effective in driving flagellar rotation, at least in a certain range of Δp. Furthermore, the rotation rate increased linearly with $|\Delta p|$ and, in *Bacillus subtilis*, saturated above 60 to 100 mV (17, 18, 30, 44); saturation was observed both for $\Delta p = \Delta\psi$ and for $\Delta p = -(kT/e_0)\Delta$pH (17).

In Fig. 7 the maximal rotation rate ν_0 is plotted as a function of Δp for two different experimental conditions. In case *a* the proton concentrations c' and c'' are equal and Δp is given by the transmembrane voltage $\Delta\psi$. In case *b*, $\Delta\psi$ is zero and Δp is entirely determined by ΔpH $= -\log(c'/c'')$. In accordance with thermodynamic expectation, the predicted rotation rates agree for small values of Δp. At larger Δp, ν_0 increases in a superlinear fashion in case *b*, whereas in case *a* the rotation rate approaches a limiting value for $-\Delta p > 50$ mV. The saturation in case *b* results from the fact that at high driving force the overall rate is limited by the intrinsic jumping frequencies of the ion which are independent of Δp for $\Delta\psi = 0$. In case *a* in which Δp is present as a transmembrane voltage $\Delta\psi$, the jumping frequencies in forward direction exponentially increase with increasing Δp (Eqs. 4 and 5), leading to a superlinear dependence of ν_0 on Δp.

In the presence of a purely electrical driving force ($\Delta p = \Delta\psi$), saturation behavior of ν_0 is predicted whenever the rate-limiting step is voltage independent. This is illustrated in Fig. 8 in which ν_0 is plotted as a function of Δp for $n = 2$. Curve *a* has been calculated assuming that all barrier heights are equal and are equally affected by voltage. Curve *b* refers to the case that the entrance barriers are rate-limiting and are insensitive to voltage. The relationship between ν_0 and Δp is superlinear in case *a* and saturating in case *b*. A dependency of ν_0 on Δp similar to curve *b*, albeit with a less pronounced saturation, is obtained when the central barrier is rate limiting and voltage insensitive.

When the motor operates at high load (close to $\nu = 0$), the equivalence between $\Delta\psi$ and ΔpH extends over a larger range of Δp. This may be expected since in the limit $\nu = 0$ the torque becomes a unique function of Δp (Eq. 23). In Fig. 9 the rotation rate ν at high viscous load ($f/kT = 20$

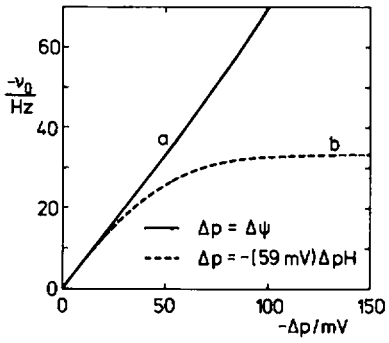

FIGURE 7 Maximal rotation rate $\nu_0 \equiv \nu$ ($M = 0$) as a function of protonmotive force Δp. Curve *a*, driving force consisting in a transmembrane voltage ($\Delta p = \Delta\psi$); curve *b*, driving force consisting in a pH difference [$\Delta p = (kT/e_0) \ln(c'/c'') = -(59\text{ mV})\Delta$pH]. Both curves have been calculated for $n = 2$ with $c' = 10^{-7}$ M; $K' = K'' = 10^{-9}$ M; $H = 1$; $\tilde{k}'_0 = \tilde{k}'_1 = \tilde{k}'_2 = \tilde{k}''_1 = \tilde{k}''_2 = \tilde{k}''_3 = k_0 = 6{,}000\ s^{-1}$; $\alpha_0 = \alpha_1 = \alpha_2 = 1/3$; $N_r = 30$. For this choice of parameters, curve *b* is given by $\nu_0 = -(k_0/6N_r)tgh(-e_0\Delta p/2kT)$.

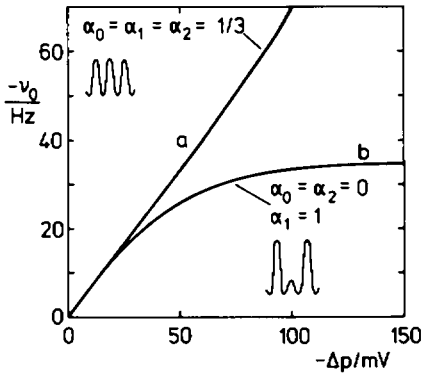

FIGURE 8 Maximal rotation rate ν_0 as a function of protonmotive force Δp under the condition $c' = c''$, $\Delta p = \Delta\psi$ (purely electrical driving force). $c' = c'' = 10^{-7}$ M; $K' = K'' = 10^{-9}$ M; $H = 1$; $N_r = 30$. Curve *a*, all barrier heights equal and equally affected by voltage ($\tilde{k}'_0 = \tilde{k}'_1 = \tilde{k}'_2 = \tilde{k}''_1 = \tilde{k}''_2 = \tilde{k}''_3 = k_0 = 6{,}000\ s^{-1}$; $\alpha_0 = \alpha_1 = \alpha_2 = 1/3$). Curve *b*, entrance barriers rate limiting and voltage insensitive ($\tilde{k}'_0 = \tilde{k}''_1 = \tilde{k}'_2 = \tilde{k}''_3 = 4{,}200\ s^{-1}$, $\tilde{k}'_1 = \tilde{k}''_2 = 10^5\ s^{-1}$; $\alpha_0 = \alpha_2 = 0$, $\alpha_1 = 1$). The values of the rate constants have been chosen such that the slopes of $\nu_0(\Delta p)$ agree at low Δp.

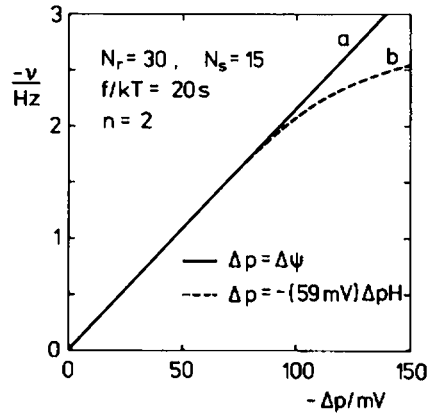

FIGURE 9 Rotation rate ν as a function of protonmotive force Δp in the limit of high viscous load ($f/kT = 20$ s). f is the rotational friction coefficient defined by $M_e = -M = f \cdot \Omega = -f \cdot 2\pi\nu$, where Ω is the angular velocity. Curve *a*, driving force consisting in a transmembrane voltage ($\Delta p = \Delta\psi$); curve *b*, driving force consisting in a pH difference [$\Delta p = -(59\text{ mV}/\Delta\text{pH})$]. Curves *a* and *b* have been obtained by calculating $M(\nu)$ from Eqs. 18 and 21, using the parameter values given in the legend of Fig. 7. $\nu(\Delta p)$ was evaluated from the intersection of $M(\nu)$ with the straight line $M = f \cdot 2\pi\nu$ for $f/kT = 20$ s.

s) is plotted as a function of Δp for $c' = c''$, $\Delta p = \Delta\psi$ (curve *a*) and for $\Delta\psi = 0$, $\Delta p = -(kT/e_0)\Delta\text{pH}$ (curve *b*). It is seen that the two curves nearly coincide up to $-\Delta p \approx 100$ mV. In contrast, at low viscous load ($\nu \approx \nu_0$) the range of Δp in which $\Delta\psi$ and ΔpH are equivalent is much smaller, as Fig. 7 shows.

Continuum Treatment of Model I: Behavior at Small Driving Forces

In this section we give a simplified treatment of the model of intersecting half-channels, assuming that the number of barriers and wells along the transport pathway is large ($n \to \infty$) so that ion movement in the channel becomes quasi-continuous. We allow the number of half-channels on the rotor (Fig. 1) to be larger than $N_r \equiv 2\pi/\phi$, but still require that a given stator half-channel can be occupied by not more than one ion at a time. When the ligand rows on the periphery of the rotor are narrowly spaced, ions may enter and leave the stator half-channels at virtually any position of the rotor, so that the stator elements become statistically independent even without elastic coupling. We further assume that the gradients of ion concentration and electric potential are small; under this condition the protonmotive force is given by (with $c' \equiv c + \Delta c$, $c'' \equiv c$):

$$\Delta p \approx \Delta\psi + (kT/e_0)\Delta c/c. \tag{31}$$

According to Eq. 2, the torque acting on the rotor by a single ion is equal to $(e_0\Delta p/h) \cdot h/\phi = e_0\Delta pN_r/2\pi \equiv m$. The total torque from all ions present in the motor is given by PN_sm, where P is the probability that a given stator half-channel is occupied by an ion:

$$P = \frac{c}{c + K_c}. \tag{32}$$

The equilibrium dissociation constant K_c depends on the number n of internal energy wells in the channel (45). When the motor rotates at a frequency ν, a frictional force of magnitude $-2\pi\nu(f + f_i)$ results. f is the frictional coefficient describing the hydrodynamic interaction of the flagellum with the medium and f_i is the intrinsic frictional coefficient of the motor which may be expressed by

$$f_i = N_s\,[Pf_i^* + (1 - P)f_i^0]. \tag{33}$$

f_i^* and f_i^0 are the contributions of the single intersection site in the occupied and in the empty state, respectively, to f_i. For the sake of generality, we assume that an additional externally applied torque M_a acts on the motor (46). When the motor runs at constant rate, the total torque, $PN_sm - 2\pi\nu(f + f_i) + M_a$, must vanish. This yields

$$\nu = \frac{PN_rN_se_o\Delta p + 2\pi M_a}{4\pi^2(f + f_i)}. \tag{34}$$

To obtain a relation between the rotation rate ν and the torque M which is generated by the motor at $M_a = 0$, we use the relation $M = 2\pi\nu f$ introduced before. This gives

$$M = M_0(1 - \nu/\nu_0) \tag{35}$$

$$M_0 = PN_rN_se_0\Delta p/2\pi \tag{36}$$

$$\nu_0 = \frac{1}{4\pi^2} \cdot \frac{PN_re_0\Delta p}{Pf_i^* + (1 - P)f_i^0}. \tag{37}$$

M_0 and ν_0 are the maximal torque and the maximal rotation rate introduced previously (Eqs. 23 and 24). Eqs. 36 and 37 hold at arbitrary ion concentration c, whereas Eqs. 23 and 24 have been derived under the condition $P \approx 1$. Eq. 35 is identical with the empirical linear relation between torque and rotation rate (Eq. 27). In general, Eq. 35, which has been derived for small protonmotive force Δp, may be expected to hold only in a limited range of Δp.

The rate J of ion flux through the motor is proportional to the rotation rate ν and to the occupancy probability P:

$$J = PN_rN_s\nu\,. \tag{38}$$

The relations for J and ν may be expressed in the form of the phenomenological equations of irreversible thermodynamics (47). Since J is equal to the number of ions translocated per unit time and since $2\pi M_a$ is the mechanical energy per revolution supplied from outside, the rate Φ of free-energy dissipation is given by

$$\Phi = J \cdot e_0\Delta p + \nu \cdot 2\pi M_a. \tag{39}$$

Accordingly, $e_0\Delta p$ and $2\pi M_a$ are the forces that are conjugated to the fluxes J and ν, respectively. From Eqs. 34 and 38 one obtains

$$J = L_{11} \cdot e_0\Delta p + L_{12} \cdot 2\pi M_a \tag{40}$$

$$\nu = L_{21} \cdot e_0\Delta p + L_{22} \cdot 2\pi M_a \tag{41}$$

$$L_{11} = \left[\frac{PN_rN_s}{2\pi}\right]^2 \frac{1}{f + f_i}; \qquad L_{22} = \frac{1}{4\pi^2(f + f_i)} \tag{42}$$

$$L_{12} = L_{21} = \frac{PN_rN_s}{4\pi^2(f + f_i)}. \tag{43}$$

Eq. 43 corresponds to Onsager's symmetry relation which generally holds at small driving forces (47).

Thermal Fluctuations of Rotation Speed

A small molecular system such as the flagellar motor is necessarily subjected to large thermal fluctuations. Statistical fluctuations of rotation speed may result from different sources. Both the membrane potential $\triangle\psi$ and the cytoplasmic proton concentration c' exhibit stochastic variations. Effects of fluctuations of $\triangle\psi$ (48) and of c' on the flagellar motor are probably small, however. (Although the average number n_p of "free" protons is small inside a bacterium, fluctuations of n_p are strongly damped by cytoplasmic buffers in the time range that is of interest here.) Another source of fluctuations is the time variation

of the number of driving ions inside the force-generating units. This results (at constant Δp) in fluctuations of the driving force acting on the motor. At nonsaturating ion concentrations the relative amplitude of occupancy fluctuations may be large (of the order of $1/\sqrt{PN_s}$), but since their correlation time is short (of the order of $1/N_r\nu$), the associated fluctuations of rotation speed of the flagellum are likely to be strongly damped by elastic filtering.

A further source of fluctuations is Brownian motion. Bacterial flagella carry out rotational diffusion that is superimposed on energy-driven rotation (39). If D_{rot} is the rotational diffusion coefficient, the variance of the rotational angle χ after a time Δt is given by (49)

$$\langle(\Delta\chi)^2\rangle = 2D_{rot}\Delta t = \frac{2kT\Delta t}{f+f_i}. \tag{44}$$

The magnitude of the effect of Brown motion may be described by the root-mean-square deviation $\delta\chi$ of rotational angle χ after one revolution:

$$\delta\chi \equiv [\langle(\Delta\chi)^2\rangle]^{1/2}_{\Delta t=\tau} = 2\pi\delta\tau/\tau. \tag{45}$$

$\tau = |1/\nu|$ and $\delta\tau$ are the mean value and the standard deviation of the rotation period, respectively. For small values of the protonmotive force Δp, the angle $\delta\chi$ is predicted to be, according to Eqs. 34 and 44:

$$\delta\chi = 2\pi\left[\frac{2kT}{PN_rN_se_0|\Delta p|}\right]^{1/2}. \tag{46}$$

This equation corresponds to Eq. 3 of Khan et al. (39). Implicit in the derivation of Eq. 46 is the assumption that Brownian motion and energy-driven rotation are independently superimposed. Experimentally, rotation of flagella is found to be remarkably regular, with values of $\delta\chi/2\pi$ of ~0.06 at $\Delta p = -76$ mV (39). According to Eq. 46, low values of $\delta\chi$ are predicted when the product N_rN_s is large. For instance, for $N_r = 30$, $N_s = 15$, $P = 1$, $\Delta p = 50$ mV, and $T = 293$ K, $\delta\chi/2\pi$ becomes 0.047. This means that steady rotation, even at low protonmotive force Δp, is achieved when the average number PN_s of ions in the motor is large.

MODEL II: CONFORMATIONAL TRANSITIONS DRIVEN BY ION FLOW

In the second model we consider the possibility that the stator element represents an ionic channel in which proton flow drives a cyclic sequence of conformational transitions. A mechanism of this kind has been proposed for the F_oF_1-type ATP synthetases of bacteria, mitochondria, and chloroplasts (50–53). Specifically we assume that the channel can exist in two conformations E′ and E″ with inward facing (E′) and outward facing (E″) proton binding site (Fig. 10). In state E′ the channel protein is separated from the M ring; upon binding of a proton from the cytoplasmic side ($E' + H_{cyt}^+ \rightarrow HE'$), the protein becomes attached to the ring. The channel may then undergo a conformational transition ($HE' \rightarrow E''H$) in which the binding site is switched from an inward-facing to an outward-facing configuration; at the same time the attachment site moves over a certain distance, so that the ring rotates by the angle ϕ in the clockwise direction (Fig. 11). Upon release of H^+ to the external side ($E''H \rightarrow E'' + H_{ext}^+$) the protein detaches from the rotor. A new cycle may start after back-transition to state E′. The sequence of protonations, deprotonations, and conformational transitions depicted in Fig. 10 is analogous to the reaction cycle proposed for the F_oF_1 ATP-synthase in which in one state

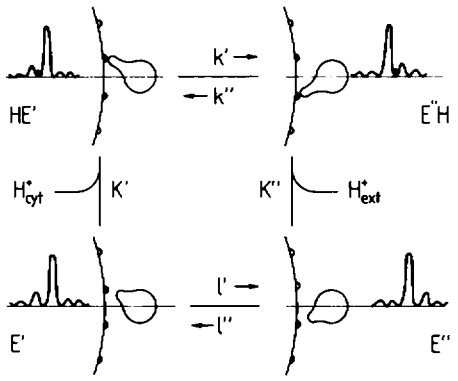

FIGURE 10 In model II the stator element is assumed to represent an ionic channel in which proton transport drives a cyclic sequence of conformational transitions. The channel can exist in two conformations E′ and E″ with inward facing (E′) and outward facing (E″) binding site. In state E′ the channel protein is separated from the M ring; upon binding of a proton from the cytoplasmic side ($E' + H_{cyt}^+ \rightarrow HE'$), the protein becomes attached to the ring. In the transition $HE' \rightarrow E''H$ the binding site is switched from an inward-facing to an outward-facing configuration; at the same time the attachment site moves over a certain distance, leading to rotation of the rotor in clockwise direction. Upon release of H^+ to the external side ($E''H \rightarrow E'' + H_{ext}^+$) the protein detaches from the ring. A new cycle may start after back-transition to state E′. The energy profile of the ion along the transport pathway inside the channel is schematically depicted for each state. In states E′/HE′ the binding site is easily accessible from the cytoplasm, but separated from the external medium by a high barrier; in states E″/E″H the site is accessible from the external side. k', k'', l', and l'' are rate constants of conformational transitions; K' and K'' are equilibrium dissociation constants of H^+.

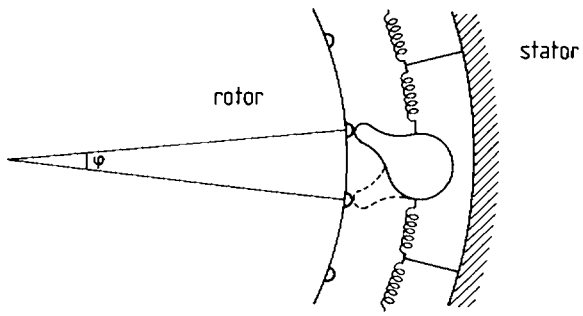

FIGURE 11 Ionic channel elastically bound to the stator. A conformational transition from state HE′ to state E″H of the channel protein leads to rotation of the rotor by the angle ϕ in the clockwise direction.

ATP is strongly bound to the protein (corresponding to the association of the channel protein with the ring), whereas in another state binding is weak so that ATP may detach from the protein (50–52).

We assume that binding of the channel protein to the ring in states HE′/E″H is strong, so that the conformational transition HE′ ↔ E″H is tightly coupled to a rotational movement of the ring. The assumption of tight coupling could be easily replaced by a more general treatment including the possibility of slippage. So far, however, the degree of coupling could not be determined experimentally. A model similar to the model considered here, but with obligatory loose coupling, has been proposed by Oosawa and co-workers (33–35). In a motor containing many channel proteins, at any given moment some channels are in the protonated, ring-attached state (HE′/E″H), so that the ring is never free to move with respect to the channel proteins. A similar situation occurs in muscle where during contraction always some of the myosin heads are attached while others are detached from the actin filament.

In the version of the model shown in Fig. 10, force is generated in the transitions HE′ ↔ E″H, clockwise rotation being associated with outward flow of protons. Switching from clockwise to counterclockwise rotation would occur if, after a cooperative transition in the structure of the ring, the ring becomes competent to bind the channel protein in states E′/E″ and to release it in states HE′/E″H.

The main difference between model II and model I is in the notion that in model I the proton interacts simultaneously with the rotor and with the stator, whereas in model II the transport pathway of H^+ is separated from the rotor, and force is transmitted from stator to rotor by a shape change of the channel protein.

In the presence of an external torque $M_e = N_s m_e$, the energy difference between states HE′ and E″H is changed by the amount w (expressed in units of kT):

$$w = \frac{m_e \phi}{kT} = \frac{2\pi M_e}{kTN_r N_s}. \tag{47}$$

$N_r = 2\pi/\phi$ is the number of attachment sites on the rotor, $N_s \leq N_r$ the number of stator elements, and m_e the torque per single stator element. In analogy to Eqs. 4 and 5, the rate constants k', k'', l', and l'' (Fig. 10) are given by

$$k' = \tilde{k}' \exp\left[(z+1)\delta u/2 + w/2\right] \tag{48}$$

$$k'' = \tilde{k}'' \exp\left[-(z+1)\delta u/2 - w/2\right] \tag{49}$$

$$l' = \tilde{l}' \exp\left(z\delta u/2\right) \tag{50}$$

$$l'' = \tilde{l}'' \exp\left(-z\delta u/2\right). \tag{51}$$

ze_0 is the electric charge of the empty ion-binding site, $u \equiv e_0(\psi' - \psi'')/kT$ the voltage in units of kT/e_0, and δ the relative dielectric distance (40) over which the binding site

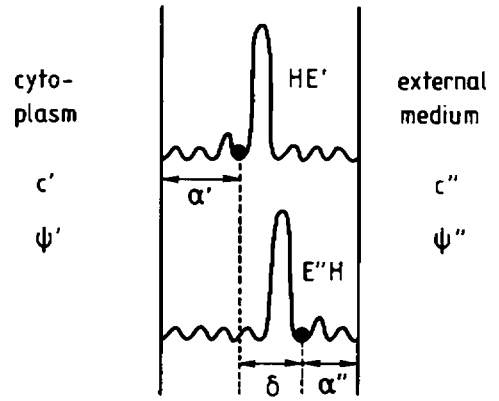

FIGURE 12 Energy profile of H^+ along the transport pathway. In conformation HE′ the ion-binding site is accessible from the cytoplasmic side, but separated from the external medium by a high energy barrier. In conformation E″H the binding site is accessible from the external medium. α', α'', and δ are dielectric distances along the transport pathway.

moves in the transition E′ ↔ E″ (Fig. 12). If part of the transmembrane voltage u drops between binding site and adjacent aqueous medium, K' and K'' become voltage dependent:

$$K' = \tilde{K}' \exp\left(-\alpha' u\right) \tag{52}$$

$$K'' = \tilde{K}'' \exp\left(\alpha'' u\right). \tag{53}$$

α' and α'' are the relative dielectric distances (Fig. 12) between binding site and water. The "ion-well" effect (41) described by Eqs. 52 and 53 represents a mechanism by which part of the transmembrane voltage becomes equivalent to a pH difference. In analogy to Eq. 11, the rate constants and equilibrium constants may be shown to be connected by

$$\frac{k'l''}{k''l'} \cdot \frac{K''}{K'} = \exp\left(u + w\right). \tag{54}$$

The proton flux j through the single stator element can be calculated using the same methods as in the analysis of model I and assuming again that protonation and deprotonation reactions are not rate limiting. If the proton concentrations c' and c'' are sufficiently high so that the empty states E′ and E″ are only weakly populated, the rotation rate ν is given by $\nu = j/N_r$ (as before). The result then reads

$$\nu = \frac{k''l'}{\sigma N_r K''}\left[c' \exp\left(u + w\right) - c''\right] \tag{55}$$

$$\sigma \equiv (1 + c'/K')(l'' + k''c''/K'') + (1 + c''/K'')(l' + k'c'/K'). \tag{56}$$

Thus, the equation for ν has a similar form as the expressions derived for model I (Eqs. 14–20). The main difference is the occurrence of terms proportional to $c'c''$ in the

denominator. This reflects the fact that at high proton concentrations transitions between the unprotonated states (E′ ↔ E″) become rate limiting.

According to Eq. 47 the torque $M = -M_e$ generated by the motor is equal to

$$M = -\frac{kT}{2\pi} N_r N_s w. \tag{57}$$

This means that the maximal torque $M_0 \equiv M(\nu = 0)$ is again given by Eq. 23.

The maximal rotation rate ν_0 at vanishing viscous load is obtained from Eq. 55 under the condition $w = 0$. This yields, together with Eq. 22,

$$\nu_0 = \frac{k''l'c''}{\sigma N_r K''} [\exp(e_0 \Delta p/kT) - 1]. \tag{58}$$

Numerical analysis of Eqs. 55–57 shows that for most combinations of the kinetic parameters, the rotation rate of ν is a nonlinear function of torque M. However, in a certain range of parameter values the function $\nu(M)$ approaches a linear behavior. (For instance, a nearly linear relationship between ν and M is obtained for $c' = c'' = 10\,K' = 10\,K''$, $\tilde{l}' = \tilde{l}'' = 10\,\tilde{k}' = 10\,\tilde{k}''$, $\alpha' = \alpha'' = 0$, $\Delta\psi = -140$ mV.) This means that model II cannot be excluded as a possible mechanism of the flagellar motor on the basis of the available experimental data.

DISCUSSION

The flagellar motor of bacteria is an osmoelectric machine (32) capable of transforming energy stored in an electrochemical potential gradient into mechanical work. The aim of this paper was to derive predictions on the dynamic properties of the motor from microscopic models. For this purpose two different mechanisms have been considered, one in which force is generated by simultaneous interaction of the driving ion with ligands on the rotor and on the stator, and one in which ion translocation induces a cycle of conformational transitions of the stator element which is coupled to motion of the rotor. Both mechanisms lead to similar predictions on the observable kinetic properties of the flagellar motor.

In the analysis of both models the assumption has been used that events in the individual force-generating units are uncorrelated. This assumption seems reasonable, since correlation between many single elements normally leads to high activation energies and to a strongly superlinear dependence of rate on driving force, which is not observed experimentally. Lack of correlation may result from elastic coupling of the stator elements to the cell wall (30, 31), or from the existence of a quasi-continuum of sites on the rotor with which the stator elements interact.

The analysis of both models leads to closed expressions describing rotation rate as a function of torque generated by the motor. The theoretical predictions are in agreement with the following experimental observations: (*a*) By measuring rotation rate ν at different viscous loads, Berg and co-workers observed a linear relationship between torque M and rotation rate (24). A linear dependence of M on ν is predicted by model I if the number of energy wells of the ion-transport pathway is sufficiently high (practically, the number of inner wells must be 2 or larger). In model II an approximately linear relationship between M and ν may be expected in a certain range of kinetic parameters. (*b*) According to Fig. 6, the rotation rate at a given viscous load should increase linearly with the number of force-generating units; this prediction, which follows directly from the assumption of independence among force generators, is consistent with the experiments of Block and Berg (10). (*c*) The torque generated by the motor at high viscous load and constant protonmotive force Δp is virtually independent of temperature (30). This agrees with Eq. 23 predicting that the maximal torque M_0 should depend exclusively on N_r, N_s, and Δp. It should be emphasized, however, that Eq. 23 is not specific to the models considered here; it may be expected to hold for any tightly coupled ion-driven motor in the limit of fully occupied binding sites. (*d*) The motor has been found to run without detectable stepping; if steps occur periodically, their number must be larger than 100 (7). In model I the number Z of steps per revolution is equal to $N_r(n + 1)$; with $N_r = 30$ and $n = 2$, Z becomes equal to 90. In model II the number of steps per revolution is given by $2\pi/\phi = N_r$; it is feasible that N_r is as large as 100. Additional smoothing of rotary motion may result from elastic filtering (31). (*e*) Both models predict that energy-driven rotation is superimposed by rotational Brownian motion, and that an intrinsic threshold value of Δp for rotation does not exist. Brownian motion at low values of Δp has been observed by Khan et al. in experiments with *Streptococcus* (39). In *Streptococcus* the threshold for rotation was found to be small, <25 mV (18). In other systems a finite threshold value of Δp for rotation was observed (17, 44). It has been proposed that in these cases the threshold may result from secondary effects, such as blocking by particulate material that gets stuck between the cell wall and the drive shaft and is expelled from the motor at a finite Δp (39). (*f*) In both mechanisms, H^+ can be replaced by other ion species, such as Na^+, which has been shown to be the driving ion for flagellar rotation in alkalophilic bacteria (21). (*g*) The reaction cycles of Figs. 3 and 10 are fully reversible. This is consistent with the finding that flagellar rotation can be driven by a protonmotive force of either sign (22, 54, 55). At a given Δp, the direction of rotation can abruptly change from clockwise to counterclockwise; by this switching reaction bacteria respond to chemosensory stimuli (2). In model I switching between clockwise and counterclockwise rotation may involve a cooperative transition in the M ring, in which the angle of inclination of the rotor half-channels is changed from θ to $-\theta$ (Fig. 1). In model II the switching mechanism may consist in a change of binding affinity of the attachment sites on the M ring with respect

to states HE'/HE" and E'/E" of the stator element (Fig. 10).

Model I and model II could be distinguished by measuring rotation rate ν as a function of the intra- and extracellular proton concentrations c' and c''. Whereas for model I a saturation behavior is predicted at large values of c' and c'' (Eqs. 14–20), the rotation rate should decrease to zero for increasing c' and c'' in model II (according to the term proportional to $c'c''$ in Eq. 56). This concentration dependence of ν in model II results from the fact that at high proton concentration, transitions between the unprotonated states E' and E" become rate-limiting.

A further experimental test of the theoretical models consists in determining the ratio of rotation rate ν and ion-flux rate J. Oosawa and co-workers (33–35) have analyzed models based on loose coupling between ν and J, in which the ratio ν/J varies with viscous load. In contrast, in the mechanisms considered in this paper, ν and J are tightly coupled and their ratio is load-independent. It should be clear, however, that tight coupling represents an idealized limiting case and that deviations from the limiting coupling ratio may occur, for instance, when in model I ions pass across barriers in the channel without a concomitant movement of the rotor.

Detailed information on microscopic properties of the flagellar motor may be obtained by measuring rotation rate as a function of voltage and of intra- and extracellular proton concentrations. Depending on the microscopic parameters of the model, the relationship between rotation rate and protonmotive force may be superlinear, linear, or saturating, as illustrated by Figs. 7–9.

APPENDIX A

Derivation of Eq. 11

We consider the case that only a single stator-element is present and that the transitions $A_0 \leftrightarrow A_1 \leftrightarrow A_2 \ldots A_n \leftrightarrow A_{n+1}$ are completely blocked. Under this condition a true equilibrium state can be established for arbitrary values of c', c'', and $\Delta\psi \equiv \psi' - \psi''$ by imposing an external torque m_e of appropriate magnitude. m_e is obtained from the condition that in the equilibrium state the change of free energy, $\Delta\tilde{\mu}_H = F\Delta\psi + RT \ln (c'/c'')$, associated with the transport of one mole of H^+ across the membrane must be equal to the mechanical work $-Lm_e\phi$ required for rotating the ring by the angle $L\phi$ (Fig. 1) against the external torque m_e (F is the Faraday constant, R the gas constant, T the absolute temperature, and L the Avogadro constant). With $RT/F = kT/e_0$, $u = e_0\Delta\psi/kT$, and $w = m_e\phi/kT$ one obtains

$$-w = u + \ln (c'/c'') \text{ (equilibrium).} \qquad \text{(A1)}$$

For the derivation of Eq. 11 we combine the equilibrium conditions

$$\frac{x[B_{i+1}]}{x[B_i]} = \frac{k_i'}{k_{i+1}''} \qquad (i = 0, 1, \ldots n) \qquad \text{(A2)}$$

with Eqs. A1, 9, and 10. This yields

$$\frac{k_0'k_1' \ldots k_n'}{k_1''k_2'' \ldots k_{n+1}''} \cdot \frac{K''}{K'H} = \exp (u + w). \qquad \text{(A3)}$$

Since any value of $u + w$ can be obtained by a suitable choice of c''/c' and since the kinetic parameters on the left-hand side of Eq. A3 are independent of c' and c'', Eq. A3 holds for equilibrium as well as nonequilibrium conditions. This proves Eq. 11.

APPENDIX B

Derivation of Eqs. 14–20

In the following we calculate the ion flux j through the single stator-channel in the limit of high ion concentrations ($c' \gg K', c'' \gg K''$). Under this condition the probability P that the channel is occupied by an ion is unity:

$$P \equiv \sum_{i=0}^{n+1} x[B_i] = 1. \qquad \text{(B1)}$$

In the steady state the time variation of the probabilities $x[B_i]$ vanishes:

$$\frac{dx[B_i]}{dt} = k_{i-1}' x[B_{i-1}] + k_{i+1}'' x[B_{i+1}] - (k_i' + k_i'') x[B_i] = 0 \qquad \text{(B2)}$$

$$(i = 1, 2, \ldots, n).$$

Eqs. B1 and B2 together with Eqs. 9 and 10 represent a system of $n + 4$ equations for the determination of the $n + 4$ unknowns $x[A_0]$, $x[A_{n+1}]$, $x[B_0], \ldots, x[B_{n+1}]$. The steady-state net flux j is obtained from any of the relations

$$j = k_i' x[B_i] - k_{i+1}'' x[B_{i+1}], \qquad \text{(B3)}$$

together with Eq. 11. j and $\nu = j/N_r$ can be easily calculated for small values of n. The results for $n = 0$, 1, and 2 are represented in Eqs. 14–20. For $n > 2$ it is more practical evaluating the unknowns $x[B_i]$ numerically by the method of matrix inversion (42).

I thank W. Boos and M. Manson for discussions and H. C. Berg and R. M. Macnab for comments to the manuscript.

This work has been financially supported by Deutsche Forschungsgemeinschaft (Sonderforschungsbereich 156).

Received for publication 30 June 1987 and in final form 16 September 1987.

REFERENCES

1. Berg, H. C. 1975. Chemotaxis in bacteria. *Annu. Rev. Biophys. Bioeng.* 4:119–136.
2. Berg, H. C. 1975. Bacterial behavior. *Nature (Lond.).* 254:389–392.
3. Silverman, M., and M. Simon. 1977. Bacterial flagella. *Annu. Rev. Microbiol.* 31:397–419.
4. Iino, T. 1977. Genetics of structure and function of bacterial flagella. *Annu. Rev. Genet.* 11:161–182.
5. Macnab, R. M. 1978. Bacterial motility and chemotaxis: the molecular biology of a behavioural system. *CRC Crit. Rev. Biochem.* 5:291–341.
6. Silverman, M. 1980. Building bacterial flagella. *Q. Rev. Biol.* 55:395–408.
7. Berg, H. C., M. D. Manson, and M. P. Conley. 1982. Dynamics and energetics of flagellar rotation in bacteria. *Proc. Symp. Soc. Exp. Biol.* 35:1–31.
8. Macnab, R. M., and S.-I. Aizawa. 1984. Bacterial motility and the bacterial flagellar motor. *Annu. Rev. Biophys. Bioeng.* 13:51–83.
9. Silverman, M., P. Matsumura, and M. Simon. 1976. The identification of the *mot* gene product with Escherichia coli lambda hybrids. *Proc. Natl. Acad. Sci. USA.* 73:3126–3130.

10. Block, S. M., and H. C. Berg. 1984. Successive incorporation of force-generating units in the bacterial rotary motor. *Nature (Lond.)*. 309:470–412.
11. DePamphilis, M. L., and J. Adler. 1971. Fine structure and isolation of the hook-basal boday complex of flagella from Escherichia coli and Bacillus subtilis. *J. Bacteriol.* 105:384–395.
12. Coulton, J. W., and R. G. E. Murray. 1978. Cell envelope associations of Aquaspirillum serpens flagella. *J. Bacteriol.* 136:1037–1049.
13. Ridgway, H. F., M. Silverman, and M. I. Simon. 1977. Localization of proteins controlling motility and chemotaxis in Escherichia coli. *J. Bacteriol.* 132:657–665.
14. Belyakova, T. N., A. N. Glagolev, and V. P. Skulachev. 1976. Electrochemical gradient of H^+ ions as a direct source of energy during bacterial locomotion. *Biokhimiya.* 41:1206–1210.
15. Manson, M. D., P. Tedesco, H. C. Berg, F. M. Harold, and C. van der Drift. 1977. A protonmotive force drives bacterial flagella. *Proc. Natl. Acad. Sci. USA.* 74:3060–3064.
16. Matsuura, S., J.-I. Shioi, and Y. Imae. 1977. Motility in Bacillus subtilis driven by an artificial protonmotive force. *FEBS (Fed. Eur. Biochem. Soc.) Lett.* 82:187–190.
17. Khan, S., and R. M. Macnab. 1980. Proton chemical potential, proton electrical potential and bacterial motility. *J. Mol. Biol.* 138:599–614.
18. Manson, M. D., P. M. Tedesco, and H. C. Berg. 1980. Energetics of flagellar rotation in bacteria. *J. Mol. Biol.* 138:541–561.
19. Ravid, S., and M. Eisenbach. 1984. Direction of flagellar rotation in bacterial cell envelopes. *J. Bacteriol.* 158:222–230.
20. Shimada, K., and H. C. Berg. 1987. Response of the flagellar rotary motor to abrupt changes in extracellular pH. *J. Mol. Biol.* 193:585–589.
21. Krulwich, T. A. 1986. Bioenergetics of alkalophilic bacteria. *J. Membr. Biol.* 89:113–125.
22. Berg, H. C. 1974. Dynamic properties of bacterial flagellar motors. *Nature (Lond.)*. 249:77–79.
23. Berg, H. C., and L. Turner. 1979. Movement of microorganisms in viscous environments. *Nature (Lond.)*. 278:349–351.
24. Lowe, G., M. Meister, and H. C. Berg. 1987. Rapid rotation of flagellar bundles in swimming bacteria. *Nature (Lond.)*. 325:637–640.
25. Adam, G. 1977. Rotation of bacterial flagella as driven by cytomembrane streaming. *J. Theor. Biol.* 65:713–726.
26. Adam, G. 1977. Model for the bacterial flagellar motor: response to varying viscous load. *J. Mechanochem. Cell Motil.* 4:235–253.
27. Läuger, P. 1977. Ion transport and rotation of bacterial flagella. *Nature (Lond.)*. 268:360–362.
28. Glagolev, A. N., and V. P. Skulachev. 1978. The proton pump is a molecular engine of motile bacteria. *Nature (Lond.)*. 272:280–282.
29. Macnáb, R. M. 1979. How do flagella propel bacteria? *Trends Biochem. Sci.* 4:N10–N13.
30. Khan, S., and H. C. Berg. 1983. Isotope and thermal effects in chemiosmotic coupling to the flagellar motor of Streptococcus. *Cell.* 32:913–919.
31. Berg, H. C., and S. Khan. 1983. A model for the flagellar motor. *In* Motility and Recognition in Cell Biology. H. Sund and C. Veeger, editors. De Gruyter, Berlin. 486–497.
32. Mitchell, P. 1984. Bacterial flagellar motors and osmoelectric molecular rotation by an axially transmembrane well and turnstile mechanism. *FEBS (Fed. Eur. Biochem. Soc.) Lett.* 176:287–294.
33. Oosawa, F., and J. Masai. 1982. Mechanism of flagellar motor rotation in bacteria. *J. Phys. Soc. Jpn.* 51:631–641.
34. Oosawa, F., and S. Hayashi. 1983. Coupling between flagellar motor rotation and proton flux in bacteria. *J. Phys. Soc. Jpn.* 52:4019–4028.
35. Oosawa, F., and S. Hayashi. 1986. The loose coupling mechanism in molecular machines of living cells. *Adv. Biophys.* 22:151–183.
36. Perez-Garcia, D. J., and J. E. Llebot. 1987. Bacterial flagellar rotation as a nonequilibrium phase transition. *J. Theor. Biol.* 122:453–458.
37. Wagenknecht, T. 1986. A plausible mechanism for flagellar rotation in bacteria. *FEBS (Fed. Eur. Biochem. Soc.) Lett.* 196:193–197.
38. Zwolinski, B. I., H. Eyring, and C. E. Reese. 1949. Diffusion and membrane permeability. *J. Phys. Chem.* 53:1426–1453.
39. Khan, S., M. Meister, and H. C. Berg. 1985. Constraints on flagellar rotation. *J. Mol. Biol.* 184:645–656.
40. Läuger, P. 1984. Thermodynamic and kinetic properties of electrogenic ion pumps. *Biochim. Biophys. Acta.* 779:307–341.
41. Mitchell, P. 1969. Chemiosmotic coupling and energy transduction. *Theor. Exp. Biophys.* 2:159–216.
42. Meister, M., and H. C. Berg. 1987. The stall torque of the bacterial flagellar motor. *Biophys. J.* 52:413–419.
43. Johnson, K. J. 1980. Numerical Methods in Chemistry. Marcel Dekker, Inc., New York. 503 pp.
44. Shioi, J.-I., S. Matsuura, and Y. Imae. 1980. Quantitative measurements of proton motive force and motility in Bacillus subtilis. *J. Bacteriol.* 144:891–897.
45. Läuger, P. 1973. Ion transport through pores: a rate-theory analysis. *Biochim. Biophys. Acta.* 311:423–441.
46. Ishihara, A., S. Yamaguchi, and H. Hotani. 1981. Passive rotation of flagella on paralyzed Salmonella typhimurium (mot) mutants by external rotary driving force. *J. Bacteriol.* 145:1082–1084.
47. Katchalsky, A., and P. F. Curran. 1967. Nonequilibrium Thermodynamics in Biophysics. Harvard University Press, Cambridge, MA. 248 pp.
48. Läuger, P. 1984. Current noise generated by electrogenic ion pumps. *Eur. Biophys. J.* 11:117–128.
49. Berg, H. C. 1983. Random walks in Biology. Princeton University Press, Princeton, NJ. 142 pp.
50. Boyer, P. D. 1975. A model for conformational coupling of membrane potential and proton translocation to ATP synthesis and to active transport. *FEBS (Fed. Eur. Biochem. Soc.) Lett.* 58:1–6.
51. Cross, R. 1981. The mechanism and regulation of ATP synthesis by F_1-ATPases. *Annu. Rev. Biochem.* 50:681–714.
52. Kozlov, I. A., and V. P. Skulachev. 1982. An H^+-ATP synthetase: a substrate translocation concept. *Curr. Top. Membr. Transp.* 16:285–301.
53. Cox, G. B., D. A. Jaus, A. L. Fimmerl, F. Gibson, and L. Hatch. 1984. The mechanism of ATP synthase: conformational change by rotation of the β subunit. *Biochim. Biophys. Acta.* 768:201–208.
54. Berg, H. C., and P. M. Tedesco. 1975. Transient response to chemotactic stimuli in *Escherichia coli*. *Proc. Natl. Acad. Sci. USA.* 72:3235–3239.
55. Khan, S., and R. M. Macnab. 1980. The steady-state counterclockwise/clockwise ratio of bacterial flagellar motors is regulated by protonmotive force. *J. Mol. Biol.* 138:563–597.